Tellus (2005), 57B, 175–188
Printed in Singapore. All rights reserved

TELLUS

“Wet/dry Daisyworld”: a conceptual tool for quantifying the spatial scaling of heterogeneous landscapes and its impact on the subgrid variability of energy fluxes

By DENNIS D. BALDOCCHI[1]*, THERESA KREBS[1]† and MONIQUE Y. LECLERC[2],
[1]*Ecosystem Science Division/Department of Environmental Science, Policy and Management, 137 Mulford Hall, University of California, Berkeley, Berkeley, CA 94720, USA;* [2]*Lab for Environmental Physics, University of Georgia, Griffin, GA 30223, USA*

(Manuscript received 26 October 2004; in final form 4 February 2005)

ABSTRACT

We modified the “Daisyworld” model of Watson and Lovelock to consider the energy balance of vegetation with differing potential to evaporate water vapour across a 2-D landscape. High-resolution spatial fields of surface temperature, latent heat exchange and net radiation are computed using cellular automata (CA). The CA algorithm considers competition between actively transpiring “wet daisies” and “dry daisies” for bare ground through temperature-dependent birth and death probabilities.

This paper examines how differences in biophysical properties (e.g. surface albedo and surface conductance) affect the composition and heterogeneity of the landscape and its energy exchange. And with high resolution and gridded spatial information we evaluate bias errors and scaling rules associated with the subgrid averaging of the nonlinear functions used to compute surface energy balance.

Among our key findings we observe that there are critical conditions, associated with albedo and surface resistance, when wet or dry/dark or bright “daisies” dominate the landscape. Second, we find that the heterogeneity of the spatial distribution of “daisies” depends on initial conditions (e.g. a bare field versus a random assemblage of surface classes). And third, the spatial coefficient of variation of land class, latent heat exchange, net radiation and surface temperature scale with the exponential power of the size of the averaging window.

Though conceptual in nature, the 2-D “wet/dry Daisyworld” model produces a virtual landscape whose power-law scaling exponent resembles the one derived for the spatial scaling of a normalized difference vegetation index for a heterogeneous savanna ecosystem. This observation is conditional and occurs if the initial landscape is bare with two small colonies of “wet” and “dry” daisies.

Bias errors associated with the nonlinear averaging of the surface energy balance equation increase as the coefficient of variation of the surface properties increases. Ignoring the subgrid variability of latent heat exchange produces especially large bias errors (up to 300%) for heterogeneous landscapes. We also find that spatial variations in latent heat exchange, surface temperature and net radiation, derived from our “Daisyworld” model, scale with the spatial variation in surface properties. These results suggest that we may be able to infer spatial patterns of surface energy fluxes from remote sensing data of surface features. “Wet/dry Daisyworld”, therefore, has the potential to provide a link between observations of landscape heterogeneity, deduced from satellites, and their interpretation into spatial fields of latent and sensible heat exchange and surface temperature.

1. Introduction

Numerical models and remote sensing instruments borne on satellites are among the tools employed by biogeoscientists to assess weather, climate and atmospheric chemistry. Numerical models calculate the time rate of change of meteorological scalars by quantifying both the fluxes of mass and energy into and out of the atmosphere and the advection across lateral and vertical boundaries (McGuffie and Henderson-Sellers, 1997; Sellers et al., 1997). These calculations hinge upon information on the composition, structure and functional capacity (e.g. minimal stomatal resistance and maximal photosynthesis rates) of the Earth’s terrestrial biosphere. Today, some information on surface structural and functional properties and flux boundary

---

*Corresponding author.
e-mail: baldocchi@nature.berkeley.edu
†Present address: Risk Management Solutions, Newark, CA.

conditions can be inferred from space (Running et al., 2004; Ustin et al., 2004), while other information is gleaned from field observations provided by ecological and micrometeorological networks (Canadell et al., 2000; Baldocchi et al., 2001).

Numerical models and many remote sensing instruments view the Earth's surface at discrete and rather coarse spatial scales. In the case of land–atmosphere models, the horizontal length scale of individual grid cells typically range between 1 and 50 km on a side for mesoscale models (Avissar, 1995; Pyles et al., 2003) and 100 to 500 km on a side for global models (Dickinson, 1995; Sellers et al., 1997). Satellite-based sensors that periodically observe the Earth's surface, like the Advanced Very High Resolution Radiometer (AVHRR) and the Moderate Resolution Imaging Spectroradiometer (MODIS), have pixel resolutions of the order of 250 to 1000 m (Running et al., 1995, 1999). Subgrid scale information, within 1 km pixels, can be obtained using higher-resolution sensors (1 to 4 m) like IKONOS (Morisette et al., 2003) or aircraft-mounted sensors like the Airborne Visible/Infrared Imaging Spectrometer (AVIRIS) (Ustin et al., 2004). But these high-resolution sensors tend to be employed to view the Earth's surface episodically rather than periodically.

Landscapes, whose horizontal dimensions correspond with the grid size of a land–atmosphere model or coarse resolution satellite sensors, are rarely uniform. Typical grid size regions are comprised of a mosaic of land patches, each with a different potential to control or influence momentum, mass and energy transfer (Raupach, 1991; Bonan et al., 1993; Pielke et al., 1998). Of prime concern is how the spatial variability of surface fluxes, within and among constituent patches of a landscape, are integrated and averaged at the scale of the model grid (Raupach, 1991; McNaughton, 1994; Raupach and Finnigan, 1995; Avissar, 1995; Bunzli and Schmid, 1998; Brunsell and Gillies, 2003; Lyons and Halldin, 2004).

To quantify the spatial average of a model's finest grid scale we must evaluate the expected value $E[\,]$ of a set of nonlinear functions that represent surface energy flux densities $F(\,)$. These functions are dependent upon independent variables a that vary across a spatial domain (x, y) and are bounded within a finite extent, denoted by X and Y. Conceptually, $E[F(a(x, y))]$ is dependent upon the integration of the function across the extent of the independent variable and weighted by its probability density function $p(a(x, y)$. This integral is then integrated across the spatial domain, X, Y, such that:

$$E[F(a(x, y))] = \int_0^Y \int_0^X \int_{-\infty}^{\infty} F(a(x, y))p(a(x, y))\,\mathrm{d}a\,\mathrm{d}x\,\mathrm{d}y. \quad (1)$$

Due to the complexity of evaluating eq. (1), it is common practice to evaluate a spatially averaged surface energy flux density, $F(\langle a\rangle)$, in terms of the spatial mean of an independent value, $\langle a\rangle$. Bias errors occur when the expected values of the spatially averaged energy flux density $E[F(a(x, y))]$ do not equal the energy flux densities evaluated as a function of the mean of the forcing variable $F(\langle a\rangle)$. The magnitude of this bias error, for a single independent variable a, can be estimated using a Taylor's expansion series, truncated at the second order:

$$E[F(a)] \approx F(\langle a\rangle) + \frac{1}{2}\frac{\partial^2 F(\langle a\rangle)}{\partial a^2}\sigma_a^2. \quad (2)$$

On inspection of eq. (2) we conclude that the bias error $E[F(a)] - F(\langle a\rangle)$ is a function of the second partial derivative of the function $F(a)$ with respect to a, and the spatial variance of the independent variable σ_a^2. In summary, the spatial average of surface energy fluxes is prone to bias when the functional representation of the energy flux density is a nonlinear function of an environmental or biological forcing variable (e.g. albedo, surface and aerodynamic resistance, humidity deficits and available energy) that possesses a non-Gaussian probability distribution in space (Brunsell and Gillies, 2003). The magnitude of this bias error will vary with the spatial resolution of the averaging domain because the spatial variance of the variable σ_a^2 is a power-law function of the size of the spatial averaging window Δ (Levin, 1992).

Real-world analysis of subgrid averaging and the assessment of flux-weight resistances (Raupach, 1991; McNaughton, 1994) is hampered due to the lack of high-resolution information on spatial variations of surface energy fluxes. Rarely, for example, do we have information on the spatial variances of λE, R_n, and H or components such as surface temperature, T_s, and the aerodynamic and surface resistances, R_a and R_s.

Tower-based eddy flux measurements produce direct measurements of energy exchange (Baldocchi, 2003) but they 'smear' the flux information that is contained within a spatial footprint of several hundred to a thousand metres square in area (Schmid, 2002). Low-level aircraft flights of flux instrumentation can produce some information on the spatial variation of energy flux densities and meteorological variables (Crawford et al., 1996; Desjardins et al., 1997; Brunsell and Gillies, 2003; Kustas et al., 2003; Lyons and Halldin, 2004). However, aircraft are flown episodically, and generally along horizontal transects. Furthermore, they act like moving towers, so they too produce a smeared view of underlying latent and sensible energy fluxes (Ogunjemiyo et al., 2003). Remote sensing instrument systems, like IKONOS, can produce high-resolution information on some surface properties (at a scale between 1 and 4 m). But remote sensing produces indirect information on surface characteristics and these are used to infer surface energy fluxes (Sellers, 1987; Brunsell and Gillies, 2003; Running et al., 2004). So most available methods—tower and airborne eddy flux measurements and high-resolution remote sensing instruments—have a limited ability to quantify the subgrid variability of surface energy fluxes.

An alternative approach to the experimental study of the subgrid scale variability of surface fluxes involves a theoretical analysis that couples models employed by landscape ecologists to simulate spatial patterns of vegetation with biophysical algorithms used by micrometeorologists. We start with the conceptual model "Daisyworld" (Watson and Lovelock, 1983) and modify it to consider latent and sensible heat exchange from vegetated surfaces. We then take this theory, which we denote "wet/dry Daisyworld", and couple it with 2-D cellular automata (CA) theory (von Bloh et al., 1999), to create 2-D energy flux fields over virtual landscapes of "wet" and "dry" daisies which differ in their albedos and surface conductances. Within these virtual landscapes, which may be spatially heterogeneous or homogeneous, we are able to compute surface temperature and sensible and latent heat fluxes explicitly and at high spatial resolution.

Our overarching goal is to use the 2-D "wet/dry Daisyworld" model to investigate theoretical questions associated with vegetation–atmosphere interactions. Key questions we address in this paper include:

(1) Are there critical values of albedo and surface resistance that cause the composition of the landscape to switch between different dominant vegetation classes?

(2) If such switches occur, how do they alter the energy exchange components of a spatially integrated surface?

(3) What are the bias errors associated with computing energy exchange over heterogeneous surfaces as a function of a mean forcing variable?

(4) Does the spatial variation of surface energy fluxes scale with spatial variation in surface properties?

Our intent is to use this information to derive theoretical scaling algorithms that may link surface properties detected with satellite-borne sensors with the surface energy fluxes they infer. In other words, we endeavour to define scaling laws that transform coarse to fine-scale information on surface heterogeneity into energy fluxes that reflect the effects of high-resolution spatial variation on aggregated energy fluxes. While this analysis is theoretical, it has relevance to our understanding of subgrid parametrization of energy exchange over heterogeneous landscapes like savannas, an ecologically important plant functional type that occupies over 20% of the terrestrial biosphere (Scholes and Archer, 1997; Baldocchi et al., 2004).

2. Theoretical background

2.1. *Daisyworld*

The "Daisyworld" model was developed by Watson and Lovelock (1983) to examine regulation of the Earth's climate by the terrestrial biosphere, as the luminosity of the sun increased over geological time. During the past 20 yr numerous authors have modified "Daisyworld" to consider additional components. For example, "Daisyworld" has been customized to consider density-dependent (Lenton and Lovelock, 2001) and interspecific competition (Cohen and Rich, 2000), competition in two dimensions (von Bloh et al., 1997, 1999; Lenton and van Oijen, 2002), mutations (Saunders, 1994) and latitudinal variations in solar insolation (Ackland et al., 2003; Adams et al., 2003). Investigators have also examined the chaotic properties of "Daisyworld" (Zeng et al., 1990) and whether or not it acts as a complex adaptive system (Lenton and van Oijen, 2002).

The original "Daisyworld" model considers competition for bare space by dark and bright vegetation, i.e. "daisies" with different albedos. The fractional area A of bright or dark "daisies" is evaluated with a simple first-order differential equation that is a function of its current state, A, and a proportionality constant, K:

$$\frac{\mathrm{d}A}{\mathrm{d}t} = K(T)A. \tag{3}$$

The proportionality constant, K, represents a balance between temperature-dependent birth, B, of "daisies" in bare spaces (A_{bare} is the fractional area of bare space) and death, d, in occupied spaces. In practice, the constant K is down-regulated as temperature gets too hot or cold and decreases as the fractional area of open space decreases:

$$K(T) = A_{\text{bare}}B(T) - d. \tag{4}$$

The birth rate B is assumed to be a parabolic function of absolute temperature T:

$$B(T) = 1 - a(T_{\text{ref}} - T)^2. \tag{5}$$

The death rate, d, is typically held constant, but it can be a function of temperature or density, too.

To quantify the time rate of change in the fractional area of the dark (A_{dark}) and bright (A_{bright}) "daisies" and bare ground (A_{bare}) three coupled differential equations are evaluated:

$$\frac{\mathrm{d}A_{\text{bright}}(t)}{\mathrm{d}t} = A_{\text{bright}}(t)[A_{\text{bare}}(t)B(T) - d(t)] \tag{6}$$

$$\frac{\mathrm{d}A_{\text{dark}}(t)}{\mathrm{d}t} = A_{\text{dark}}(t)[A_{\text{bare}}(t)B(T) - d(t)] \tag{7}$$

$$A_{\text{bare}} = 1 - A_{\text{bright}} - A_{\text{dark}}. \tag{8}$$

The albedo of the Earth, α, is computed as an area-weighted function of the dark and bright daisies and bare ground:

$$\alpha = A_{\text{dark}}\alpha_{\text{dark}} + A_{\text{bright}}\alpha_{\text{bright}} + A_{\text{bare}}\alpha_{\text{bare}}. \tag{9}$$

The surface temperature of the Earth, T_{earth}, is computed by assuming there is a radiative balance between net incoming solar radiation and the long-wave energy lost:

$$\sigma T_{\text{earth}}^4 = \frac{LS_0}{4}(1 - \alpha). \tag{10}$$

In eq. (10), L is the sun's relative luminosity, which is allowed to change over geological time, and S_0 is the sun's energy flux density (solar constant) at the top of the atmosphere (1365 W m^{-2}). The factor of 4 is introduced because the Earth's disc intercepts sunlight, but its entire surface radiates energy ($\pi r^2/4\pi r^2$). Finally, σ is the Stefan–Boltzmann constant (5.67×10^{-8} J m^{-2} K^{-4} s^{-1}).

To compute the Earth's temperature, "Daisyworld" evaluates the sum of long-wave energy loss for each component of the surface ($L\uparrow$):

$$L\uparrow = \sum \sigma A_i T_i^4. \tag{11}$$

This requires that we evaluate the surface temperature of each component

$$T_{\text{dark}}^4 = \frac{LS_0}{4\sigma}(\alpha - \alpha_{\text{dark}}) + T_{\text{earth}}^4 \tag{12}$$

$$T_{\text{bright}}^4 = \frac{LS_0}{4\sigma}(\alpha - \alpha_{\text{bright}}) + T_{\text{earth}}^4. \tag{13}$$

2.2. *Wet/dry Daisyworld*

In real ecosystems, leaves transpire and convect heat, causing the surface temperature of a moist system to differ considerably from that of a dry system (Monteith and Unsworth, 1990). To account for the effects of latent and sensible heat exchange on the surface energy balance we expanded the representation of the surface energy balance that is within "Daisyworld". The approach computes latent and sensible heat exchange of the vegetation and soil explicitly, by coupling the surface energy balance with algorithms for sensible and latent heat exchange that are based on Ohm's law; energy flux densities are proportional to the potential difference in the scalar and are inversely proportional to the sum of resistances. The formal derivation produces quadratic formulae for latent heat exchange, $a + b\lambda E + c\lambda E^2$, and surface temperature, $d + eT_s + fT_s^2$, that we solve analytically (Paw and Gao, 1988; Baldocchi et al., 1999). We then specify surface resistances and albedos for the "wet" and "dry" daisies, respectively, and specify whether the soil is wet or dry, dark or bright. Details of the energy balance computations are shown in the Appendix.

2.3. *Two-dimensional Daisyworld*

Horizontal competition for bare spaces by "wet" and "dry" daisies is computed using CA (von Bloh et al., 1997). CA computation schemes originated in the 1950s and 1960s with John von Neumann and J. H. Conway (Gardner, 1971). CA models are rule-based and have reaction–diffusion properties similar to those simulated with sets of partial differential equations (Cronhort, 2000). Consequently, they are able to generate complex spatial patterns and produce scaling properties that mimic those observed in nature (Fernandez-Illescas and Rodriguez-Iturbe, 2004; Rietkerk et al., 2004).

The computational domain is defined by a matrix of 512 by 512 cells in size. We evaluate the temporal dynamics of each cell in the domain on the basis of von Neumann's neighbourhood (a five-cell neighbourhood, consisting of a central cell and four orthogonal neighbours; alternatively one can implement Moore's neighbourhood which considers orthogonal and diagonal neighbours (Wolfram, 2002)).

The set of rules that determine the fate of each cell is probabilistic. If a cell is bare, we call a random number generator and compare the random number with the probability of birth. If the birth rate $B(T)$ exceeds the random number, then a "daisy" is born. The composition of the "daisy" in the central cell assumes the identity of one of its adjacent neighbours, chosen at random. If a cell is occupied, it either remains the same or dies. Death is decided by comparing another random number with the probability of death. Our computations are based on a random number algorithm that repeats a random sequence only once in 2^{31} calls (Press et al., 1988).

We used a Gaussian curve to describe the probability of birth (Lenton and Lovelock, 2001). This function depends on absolute surface temperature, T, it peaks at 295.5 K and equals zero at 273 and 313 K. Its functional form is:

$$B = \exp\left[-0.01(295.5 - \mathrm{T})^2\right]. \tag{14}$$

We assume that the probability of death is an exponential function of temperature that ranges between 0 and 1 as absolute surface temperature increases from 273 to 315 K:

$$d = \exp[50(\mathrm{T} - 315)/315]. \tag{15}$$

We also consider density-dependent death. The "daisy" in a central cell dies if all four adjacent neighbouring cells are occupied with similar daisies.

After the identity of the cell is determined, we assign it properties (i.e. albedo and surface resistance) that correspond to its class and then compute its surface energy balance. The whole domain is updated in a synchronous manner; the state of adjacent cells is associated with its state during the previous time-step, as opposed to an asynchronous approach that consists of new and old neighbouring cells as one marches across the grid domain). This version of "wet/dry Daisyworld" does not consider lateral advection of heat between cells. Across patches of vegetation, net lateral energy exchange is typically small compared with the vertical energy exchange across vegetation edges (Baldocchi and Rao, 1995; Park and Paw, 2004). And at the landscape scale, many studies indicate that the checkerboard approach to assessing subgrid variability of energy exchange has merit because horizontal energy advection is secondary compared with vertical energy exchange when the scales of the heterogeneous patches are smaller than the depth of the planetary boundary layer, e.g. 1 to 3 km (Raupach, 1991; Bunzli and Schmid, 1998). Nevertheless, this model framework can be adapted to consider lateral advection, as has been done by others at global scales (Adams et al., 2003). This model framework also has the flexibility to consider (1) feedbacks between energy exchange and the diurnal development of the planetary boundary layer, (2) the effects of aerodynamically smooth and rough "daisies" and (3) the effects of varying soil heat flux for vegetated and bare cells.

Table 1. Values of albedo, α, and surface resistance, R_s, assigned to wet and dry “daisies” and the bare ground for the reference case

Parameter	Wet “daisies”	Dry “daisies”	Bare ground
α	0.15	0.15	0.25
R_s (s m^{-1})	50	1000	2000

Table 2. Meteorological conditions assigned to the reference cases. Variables include solar radiation R_g, air temperature T_{air}, vapour pressure e_a, soil heat flux density G_{soil} and wind speed u

Metric	value
R_g (W m^{-2})	341
T_{air} (°C)	25
e_a (kPa)	0.1
G_{soil} (W m^{-2})	50
u (m s^{-1})	3

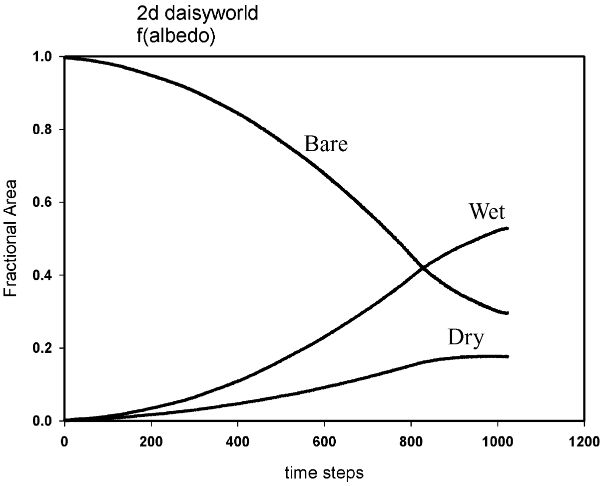

Fig. 1. Time change in bare, wet and dry fractional area of “daisies” for assorted combinations in albedo and surface resistance. These computations pertain to the case when the initial field was bare, except for clumps of vegetation in each corner of the 2-D domain.

Two initial conditions are considered in this paper. One condition seeds the initial model domain randomly with wet, bare and dry “daisies”. The other initial condition assumes that all spaces in the domain are bare, except for patches in the diagonal corners; one corner contains a cluster of wet “daisies” and the other corner contains a cluster of dry “daisies”. The first initial condition is analogous to gap dynamics that are associated with closed forest stands. The second initial condition is analogous to the regeneration of a landscape after a disturbance, like fire or logging.

Tables 1 and 2 list the parameter values and meteorological conditions that were used for the reference model runs. The flux density of solar radiation represents the mean value incident to the Earth (1365 W m^{-2}/4). This value also approximates the daily mean value for a typical mid-latitude site during summer, $\overline{R_g}$, whose maximum value approaches 1070 W m^{-2} and the daily course of which approximates a sinusoidal function, $\overline{R_g} = R_{g,max}/\pi$.

Preliminary tests were conducted to examine the numerical stability of the computational system. The CA model was run until the change with time of the fractional area of bare cells was equal to zero. For the initial condition when most cells are bare, equilibrium typically occurs after 800 to 1200 time-steps (Fig. 1). For the initial condition that consists of a random distribution of “wet”, “dry” and bare cells, only 20 to 50 iterations are needed to achieve equilibrium.

3. Results

3.1. The roles of albedo and surface resistance on the composition of Daisyworld

The relative proportion of wet and dry “daisies” and bare soil, at steady-state conditions, depends upon the surface parameters assigned to both “daisies” and bare soil, as well as the initial meteorological conditions. For example, varying the albedo of the dry “daisies” has a nonlinear impact on the fractional areas occupied by wet and dry “daisies” at equilibrium (Fig. 2). When the dry “daisies” are relatively dark (α < 0.5), the wet “daisies” dominate the population, for both sets of initial conditions. As the surface becomes brighter (α > 0.5), the fraction of wet “daisies” decreases and the dry fraction increases if the initial matrix consists of randomly distributed vegetation. In contrast, wet “daisies” out-compete dry “daisies” for the range of albedo values if the initial field is bare and dark. This behaviour also holds if we vary the albedo of the wet “daisies” (data not shown).

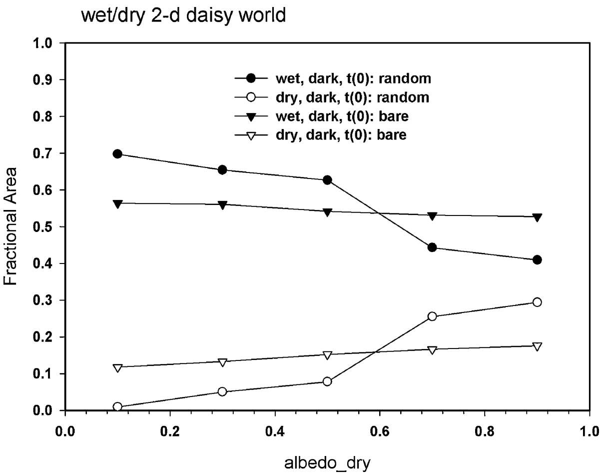

Fig. 2. The fractional area of wet and dry “daisies”. Computations were performed by varying the albedo of the dry “daisy” class. Computer runs were made for the case when the initial field was bare and when it was randomly seeded with wet and dry “daisies” and bare soil.

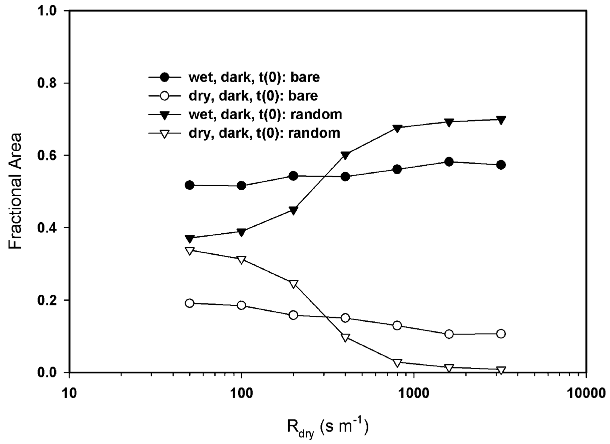

Fig. 3. The fractional area of wet and dry "daisies". Multiple computations were performed varying the surface resistance of the dry "daisy" class. Computer runs were made for the case when the initial field was bare and when it was randomly seeded with wet and dry 'daisies and bare soil.

Causing the dry "daisies" to become increasingly wetter, by reducing their surface resistance, significantly alters the proportion of wet and dry "daisies" if the initial field is seeded randomly (Fig. 3). As R_s(dry) drops below 800 s m^{-1} the spatial field changes from being dominated by wet "daisies" (>70%) to a field that has an even mix of "wet" and "dry" daisies. This switch does not occur when the initial conditions are bare, as would occur when a landscape is disturbed by fire or logging. In the second case, wet, dark "daisies" dominate the spatial field for all combinations of competing dry "daisies".

Varying the combination of albedo and the resistance of the wet "daisies" produces a different proportion of wet and dry "daisies" (Fig. 4). If the initial field is random, we find that wet, dark "daisies" dominate dark dry "daisies" in an increasing fashion as R_{wet} increases. For the alternative situation, an increase in R_{wet} causes the fraction of wet, dark "daisies" to decrease and the fraction of dry, bright "daisies" to increase. We also observe that dry, bright "daisies" dominate the spatial domain when R_{wet} is greater than 1000 s m^{-1}. In this situation, the specification of albedo overrides that of surface resistance.

Because the birth and death rates are nonlinear functions of surface temperature, varying the air temperature has a marked impact on the competition between the two classes for space. The populations of wet and dry "daisies" comprise less than 50% of the land area for cool temperatures ($T_{\mathrm{air}} \leq 10$°C). At temperatures greater than 10°C the landscape is dominated by wet "daisies" until the air temperature reaches 35°C (Fig. 5), then the populations of both wet and dry "daisies" plummet.

3.2. *Two-dimensional Daisyworld*

The CA version of "Daisyworld" produces complex spatial patterns in surface class, latent heat exchange and surface temperature. The spatial field of latent heat exchange, for example, exhibits coherent fields, associated with interconnected paths of similar vegetation and surface properties (Fig. 6). Qualitatively, the spatial field shown in Fig. 6 resembles a savanna (see Section 4) and the spatial fields computed with other CA savanna models (Jeltsch et al., 1996; von Bloh et al., 1999; van Wijk and Rodriguez-Iturbe, 2002; Fernandez-Illescas and Rodriguez-Iturbe, 2004; Rietkerk et al., 2004).

To quantify the geostatistical features of the 2-D energy flux and scalar domains we compute the spatial coefficient of

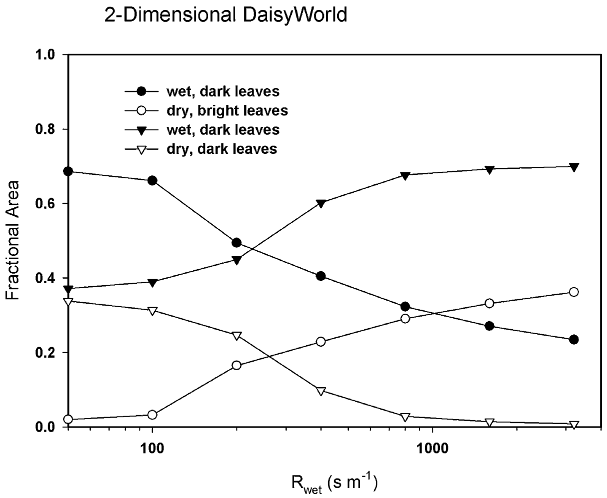

Fig. 4. The fractional area of wet and dry "daisies". Multiple computations were performed varying the surface resistance of the wet "daisy" class and by assuming either low (0.15) or high (0.75) reflectivity for the dry "daisies". Computer runs were made for the case when the initial field was randomly seeded with wet and dry "daisies" and bare soil.

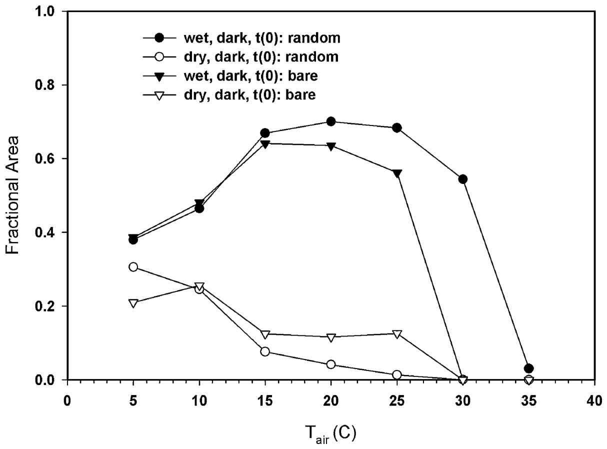

Fig. 5. The fractional area of wet and dry "daisies". Multiple computations were performed varying the air temperature of the domain. Computer runs were made for the case when the initial field was bare and when it was randomly seeded with wet and dry "daisies" and bare soil.

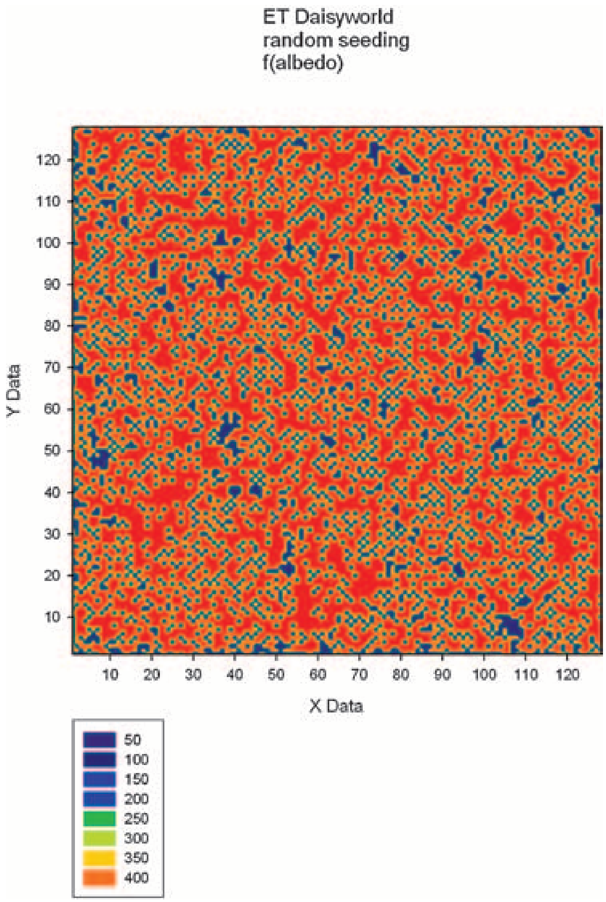

Fig. 6. Visualization of the 2-D field of latent heat exchange (W m^{-2}). This case assumed an initial field that was random.

variation for cell classification, latent heat exchange and surface temperature as a function of an averaging window, Δ (Figs. 7, 8a and 8b). In general, a log–log function describes the relationship between the dependent (the spatial coefficient of variation) and the independent (size of the averaging window) variables as long as the length scale of the window is less than the integral correlation length scale of the spatial field (Levin, 1992):

$$\log\left(\frac{\sigma_a}{E[a]}\right) = b_0 + b_1 \log(\Delta). \tag{16}$$

In eq. (16), b_0 is the intercept and b_1 is the regression slope. The log transformation of eq. (16) produces a power-law relationship where the regression coefficient, b_1, corresponds to the power-law exponent:

$$\frac{\sigma_a}{E[a]} = 10^{b_0}\Delta^{b_1}. \tag{17}$$

For reference, a spatial field is random when $\sigma_a^2/E[a]$ is equal to 1, it has a regular distribution when $\sigma_a^2/E[a]$ is less than 1 and it is clumped when $\sigma_a^2/E[a]$ is greater than 1 (Nilson, 1971). In principle, the power-law exponent approaches zero as the degree of spatial correlation increases, as in a homogeneous field, and

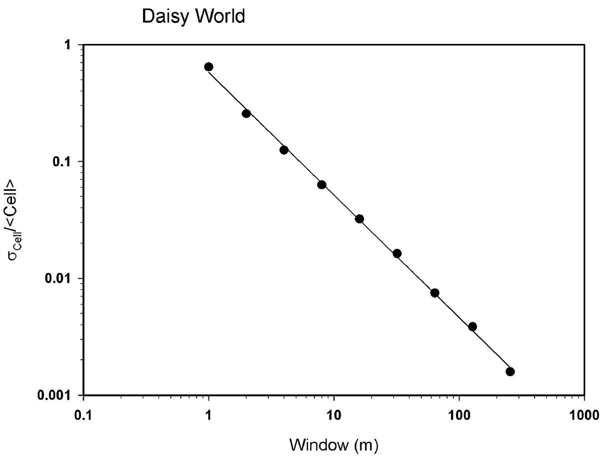

Fig. 7. Scaling of the coefficient of variation of cell class (wet, dry or bare vegetation) with the size of the averaging window. To compute spatial means and variances, wet cells were coded as 0, dry cells were coded as 1 and bare cells were assigned a value of 2. The data are plotted on a log–log scale.

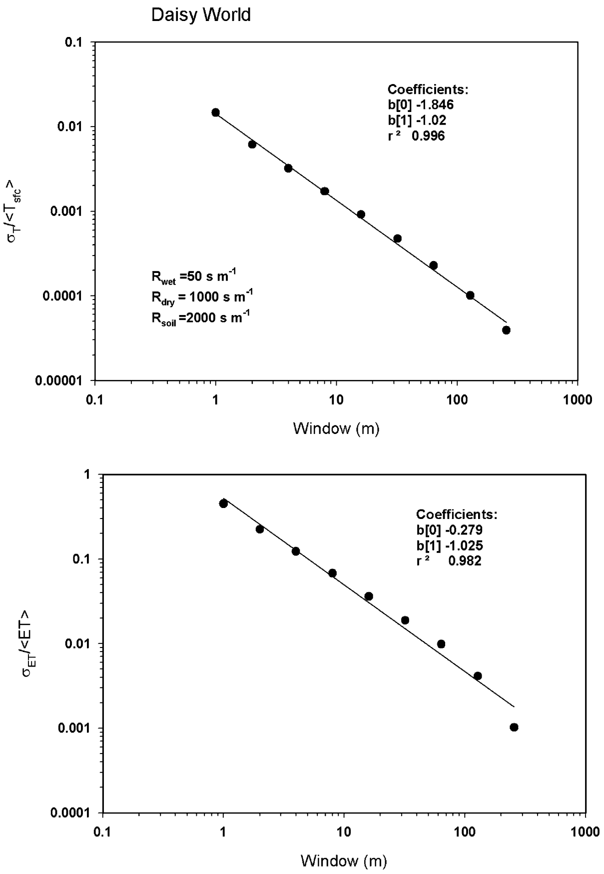

Fig. 8. The scaling of the spatial coefficient of variation of a surface temperature (a) and latent heat exchange (b) as a function of the averaging window. These computations were for the reference case (Tables 1 and 2).

it approaches −1.0 as the spatial correlation approaches zero, as with a random field (Levin, 1992).

We quantify the spatial variation in vegetation class by assigning cells with wet leaves a value of zero, cells with dry leaves a value of 1 and bare soil a value of 2 (Fig. 7). The spatial coefficient of variation of cell identity has a power-law dependency on the averaging window size. For this case, windowed-averaging (1 to 256 m) produces a power-law exponent of −1.05. The coefficient of variation, derived from assigning numerical values to the wet, dry and bare cells, decreases from 58%, when a 1 m averaging window is used, to about 0.15%, when a 256 m averaging window is employed.

A power-law scaling function also describes how the spatial coefficient of variation of surface temperature and latent heat exchange changes with size of the averaging window. For this case, the power-law exponent is −1.02 when the coefficient of variation for surface temperature or latent heat exchange is the dependent variable. From these functions we deduce that that the coefficient of variation at 1 m resolution is 1.4% for absolute surface temperature and 52% for latent heat exchange. How the power-law exponents vary with other biophysical conditions and surface heterogeneity will be investigated in more detail below.

3.3. *Spatial averaging of energy fluxes and surface temperature and subgrid variability*

We pooled calculations from sensitivity studies shown above, and others, to examine the bias errors that are associated with the subgrid averaging of the spatial fields for λE, T and R_{net}. For the virtual landscapes simulated with “Daisyworld”, we observe large bias errors in estimating latent heat exchange (Fig. 9a). On average, the mean latent heat flux is 154% greater than the expected value of latent heat exchange for the 2-D domain for the combination of variations in albedo and surface resistances of the wet and dry leaves. The magnitude of the relative bias error, however, is conditional on the spatial coefficient of variation of latent heat exchange (Fig. 9b), a reflection of the proportion and spatial variation of wet and dry “daisies”. In general, the relative error term increases in magnitude in a nonlinear fashion as the spatial coefficient of variation (cv) in λE increases. For highly heterogeneous landscapes (cv approaching 1), we observe that the relative bias error approaches 300%. For more homogeneous landscapes (cv ranging between 0 and 0.4), the relative bias error ranges between zero and 100%.

Bias errors associated with the evaluation of surface temperature are not as severe as those associated with λE. On average, we calculate a 3.5 K bias error in surface temperature, relative to its expected value (Fig. 10a). This error is similar in magnitude with direct observations over heterogeneous land surfaces (Brunsell and Gillies, 2003; Kustas et al., 2003). Overall, the relative bias error increases from zero to 2.5% as the spatial coefficient of variation of surface temperature increases from zero to 2.5%. While a 4 K bias error represents a 1 to 2% relative error in terms of absolute temperature it has significant consequences on the assessment of the surface energy budget and latent heat exchange. This is because several components of the Penman–Monteith equation are nonlinear functions of surface temperature. For example, the long-wave emission is a function of surface temperature to the fourth power and the saturation vapour pressure is an exponential function of surface temperature. Consequently, a 1% error in surface temperature (at 300 K), for example, will produce a 4% error in long-wave energy emission.

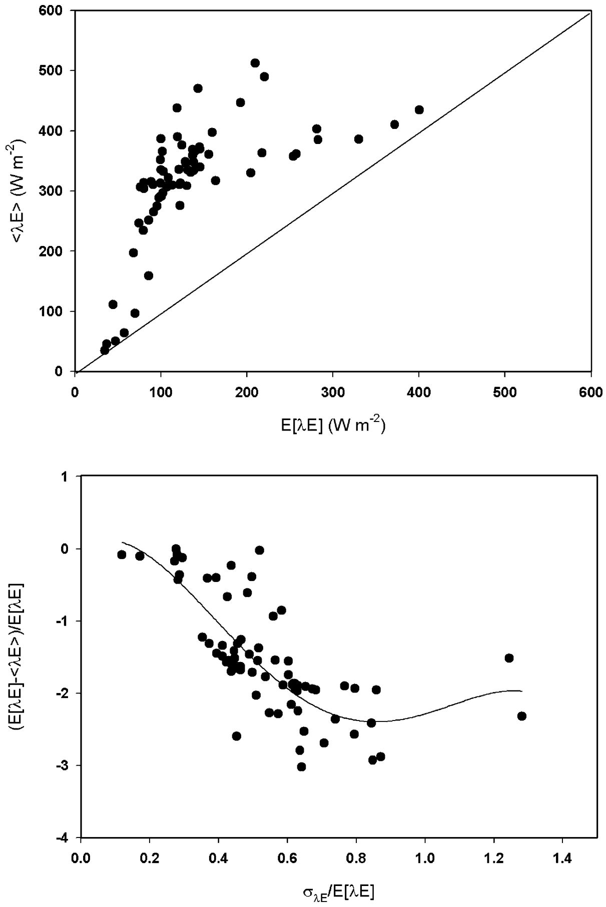

Fig. 9. (a) A comparison between the expected value latent heat exchange, $E[\lambda E]$, across a 512 by 512 pixel domain and the functional evaluation of latent heat flux, $\langle \lambda E \rangle$, computed on the basis of spatial mean albedo and surface resistance. (b) A comparison between the spatial coefficient of variation of latent heat exchange and the relative bias error.

Because bias errors in surface temperature affect long-wave energy emission, they should produce bias errors in the computation of the net radiation budget, too. On average we observe a −7.5% difference between the expected value of R_n and the value determined from averaged subcomponents like albedo, surface temperature and surface resistance (Fig. 11a). Here too, we observe that the magnitude of the relative bias error is

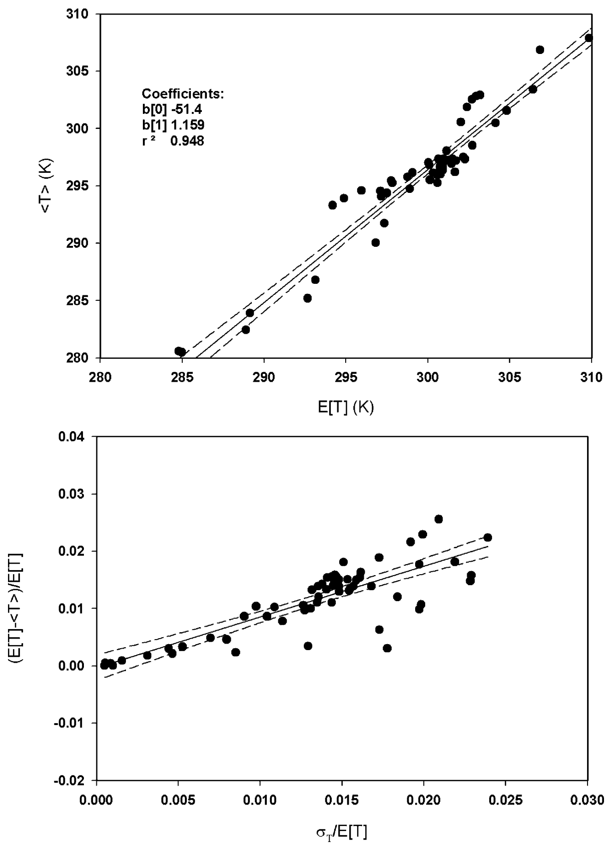

Fig. 10. (a) A comparison between the expected value of surface temperature, $E[T]$, and the mean surface temperature computed from inverting the surface energy balance in terms of mean albedo, surface resistance and net radiation, $\langle T\rangle$. (b) A comparison between the spatial coefficient of variation of surface temperature and the relative bias error.

conditional on the spatial coefficient of variation of the net radiation field; it increases from zero to 14% as the independent variable increases to 12% (Fig. 11b). Considering that many field sites do not observe energy balance closure (Wilson et al., 2002), it is feasible to expect non-representative spatial sampling of the net radiation field within the flux footprint to contribute towards this imbalance (Kim et al., 2005).

4. Discussion

There continues to be considerable debate about the relative importance of biophysical controls versus disturbance in determining and maintaining the heterogeneous structure of savannas. Ecohydrologists invoke the role of niche separation associated with trees tapping deep water sources and grasses tapping shallower water sources (Eagleson, 1982; Rodriguez-Iturbe et al., 1999). Ecologists, on the other hand, argue that disturbance from fire and grazing and their impact on subsequent recruitment dynamics cause savanna to be sparse (Jeltsch et al., 1996; Scholes and Archer, 1997; Higgins et al., 2000; Sankaran et al., 2004). Our "Daisyworld" model has the potential to investigate how a combination of factors, including the initial conditions and the biophysical properties of competing functional types, may influence the spatial heterogeneity of a savanna. In the following text, we use our model calculations to draw some new, but limited, perspectives on this debate.

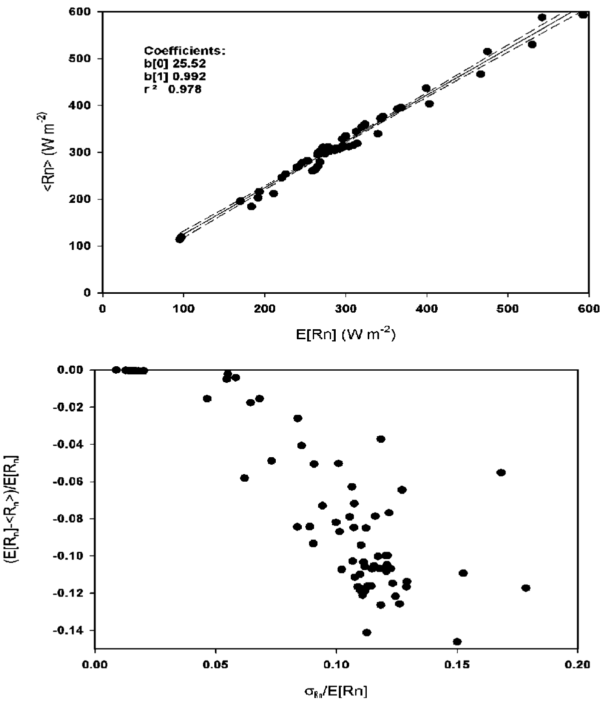

Fig. 11. (a) A comparison between the expected value net radiation, $E[R_n]$, across a 512 by 512 pixel domain and the net radiation flux computed on the basis of mean albedo and surface temperature, $\langle R_n\rangle$. (b) A comparison between the spatial coefficient of variation of latent heat exchange and the relative bias error.

First, we note that the spatial pattern of the virtual landscape created with CA has many visual similarities, such as clumping of vegetation and gaps that are observed with a panchromatic image of an oak–grass savanna in California (Fig. 12). Second, we can demonstrate a quantitative similarity between the spatial fields generated by Daisyworld and with those for the savanna using multispectral IKONOS data. This is achieved by computing the normalized difference vegetation index (NDVI) for the landscape shown in Fig. 12 and evaluating how the coefficient of variation in NDVI scales with the size of averaging window. Our computations yielded a power-law exponent of -0.2 (Fig. 13). This value is nearly identical to the exponent for virtual fields we produce with "Daisyworld" when the initial condition was bare and colonized with "daisies" in opposite corners of the grid, a condition analogous to a disturbance. In this case patchiness arises from initial disturbance and from low probabilities for birth due to unfavourable energy balance conditions associated

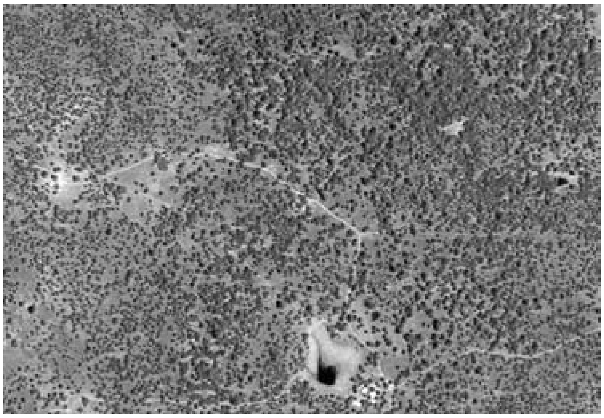

Fig. 12. Panchromatic IKONOS image (1 m resolution) of an oak–grass savanna near Ione, CA. The scale of the image is 1 km.

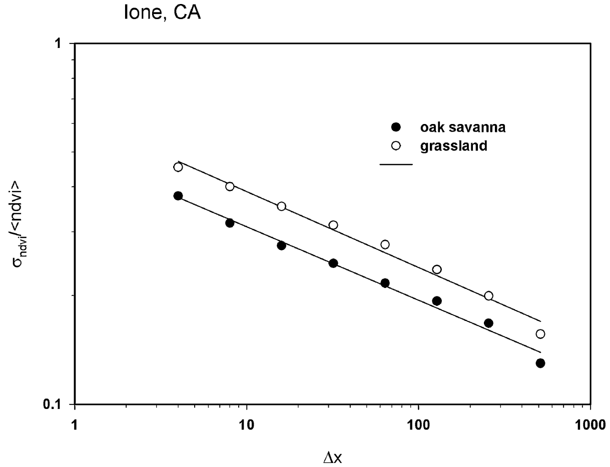

Fig. 13. Scaling relationship between the coefficient of variation of NDVI and an averaging window for an IKONOS scene of an oak–grass savanna and an open grassland growing near Ione, CA.

with bare patches. To expand upon the investigation of the causes and effects of savanna spatial patterns further and more conclusively with our "wet/dry Daisyworld" we will need to simulate the differential supply and demand for water by trees and grasses, following van Wijk and Rodriguez-Iturbe (2002), simulate the feedback between water balance and leaf area index (Baldocchi and Meyers, 1998) and consider the effects of soil temperature and moisture and grazing and fire on seedling recruitment.

Assuming we can characterize the scaling power law for surface characteristics, can this information be used to infer the spatial variation in surface energy fluxes and surface temperature? The answer to this question is yes, based on data shown in Figs 14 and 15. We observe that a linear relationship exists between the power-law exponents for the coefficient of variation associated with cell class and those associated with latent energy exchange and surface temperature, respectively. However, separate linear relations hold for the homogeneous and heterogeneous canopies; exponents near −0.2 are associated with the bare initial condition and exponents near −1.0 are generally associated with the initial condition that is composed of a random assemblage of vegetation and bare ground.

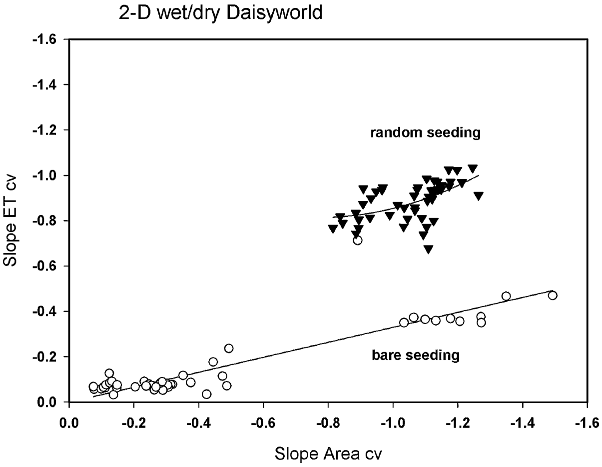

Fig. 14. Relationship between the power-law exponent for the spatial scaling of surface character and that for latent heat exchange. The power-law exponents were derived from the slopes of the log–log relation between the coefficient of variation (cv) and the size of the averaging window.

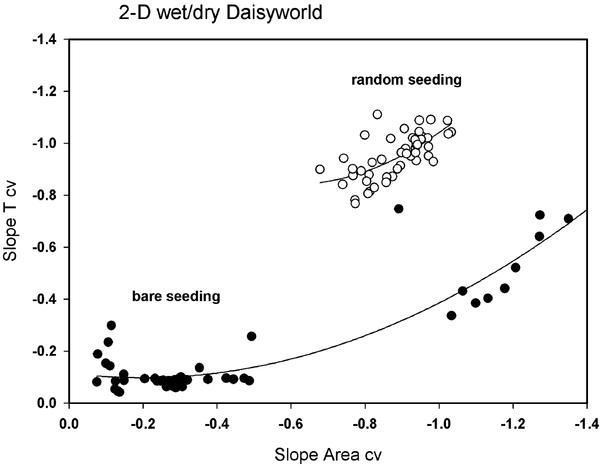

Fig. 15. Relationship between the power-law exponent for the spatial scaling of surface character and that for surface temperature. The power-law exponents were derived from the slopes of the log–log relation between the coefficient of variation (cv) and the size of the averaging window.

Finally we show there is potential to use spatial information about surface characteristics and surface temperature to infer the spatial variation in energy exchange. In Fig. 16 we observe a strong correlation between scaling power-law exponents of surface temperature and latent heat exchange (the regression slope is near 1 and the coefficient of determination, r^2, equals 0.95). These theoretical calculations support conclusions drawn

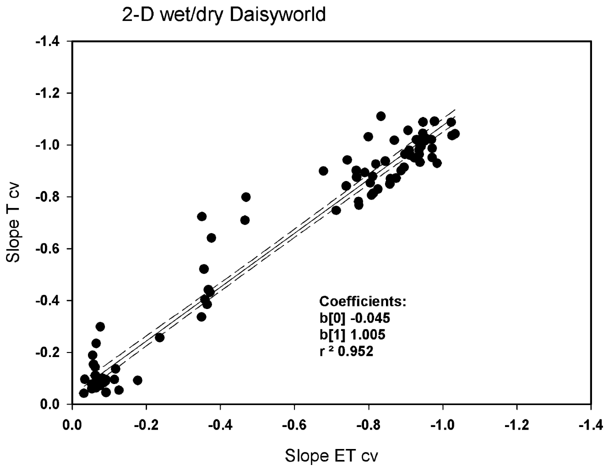

Fig. 16. Relationship between the power-law exponent for the spatial scaling of evaporation and that for surface temperature. The power-law exponents were derived from the slopes of the log–log relation between the coefficient of variation (cv) and the size of the averaging window.

by Brunsell and Gillies (2003) who report that remote sensing can be used to infer surface energy fluxes based on model calculations and aircraft overflight data.

5. Conclusion

By modifying "Daisyworld" to examine differential evaporation from different vegetation classes and soil, and coupling the energy balance model with a 2-D CA scheme that considers competition between wet and dry "daisies" we are able to produce virtual landscapes that possess similar scaling power-law exponents, describing spatial variation in structure and function, as real savannas. Since we are able to assess surface energy fluxes and surface temperature at high and low resolution, this conceptual model proves useful for testing ideas about bias errors associated with subgrid averaging and using remote sensing information on the spatial patterns of surface properties to infer how surface energy fluxes will vary in space. This analysis produces both bad and good news on these topics. First, we give the bad news which is associated with bias errors and subgrid averaging. We find that ignoring subgrid variation associated with latent heat exchange can produce huge bias errors, often exceeding 100% and sometimes approaching 300% for heterogeneous landscapes. The bias errors, however, diminish as the spatial coefficient of variation approaches zero. In contrast, bias errors are much smaller for net radiation and surface temperature. The good news deduced from this study is that spatial variation in surface properties (quantified by the power-law exponent of the plot between the coefficient of variation and the size of the averaging window) scales directly with those for latent heat exchange and surface temperature. This analysis lends credence to the concept that spatial patterns of energy exchange can be inferred with information on spatial patterns of surface properties. This version of "Daisyworld" has the potential to be a tool for providing a linkage between observations of landscape heterogeneity, deduced from satellites, and their interpretation into spatial fields of latent and sensible heat exchange and surface temperature.

In future work we intend to couple these algorithms with the growth of the planetary boundary layer and compute temporal changes in air temperature and moisture. We also intend to simulate spatial patterns in soil moisture and examine a feedback between soil moisture deficits and stomatal closure. There is also the need to examine more sophisticated competition models and consider the effects of disturbance, grazing and fire, other factors that have been hypothesized to form savannas and heterogeneous landscapes (Rietkerk et al., 2004).

6. Acknowledgments

This project was supported by a contract let by a grant from the US Department of Energy Terrestrial Carbon Project to the University of Georgia (Professor Monique Leclerc, Principal Investigator, RD316-29817513417) and the California Agricultural Experiment Station. The IKONOS image was obtained via the support of NASA for the FLUXNET project.

We thank Dr Alexander Knohl and the anonymous referees for constructive reviews of this manuscript.

7. Appendix A: Quadratic solutions for latent heat exchange and surface temperature

Latent heat exchange (λE in W m^{-2}) and surface–air temperature differences (ΔT in K) were computed analytically by solving quadratic equations associated with these dependent variables (Paw and Gao, 1988):

$$a\lambda E^2 + b\lambda E + c = 0 \tag{A1}$$

$$d\Delta T^2 + e\Delta T + f = 0. \tag{A2}$$

The coefficients $a \ldots f$, associated with the quadratic eqs (A1 and A2), can be derived through the algebraic manipulation of a set of equations describing the surface energy balance. This derivation starts with the definition of available energy, the sum of net incoming short- and long-wave energy (Q in W m^{-2}):

$$Q = R_\mathrm{g}(1-\alpha) + \varepsilon L\downarrow. \tag{A3}$$

In eq. (A3), R_g is the flux density of incoming short-wave solar radiation (W m^{-2}), α is albedo, $L\downarrow$ is the flux density of incoming long-wave radiation (W m^{-2}) and ε is emissivity. Next we define the flux density of net radiation as the balance between Q and the long-wave energy emitted by the surface, which is a function of its temperature (T_s) to the fourth power:

$$R_\mathrm{n} = R_\mathrm{g}(1-\alpha) + \varepsilon L\downarrow - \varepsilon\sigma T_\mathrm{s}^4. \tag{A4}$$

In eq. (A4) σ represents the Stefan–Boltzmann constant. At the landscape scale, net radiation is consumed via sensible, H, latent, λE, and soil, G_{soil}, heat exchange:

$$R_{\mathrm{n}} = H + \lambda E + G_{\mathrm{soil}}. \tag{A5}$$

Sensible and latent heat flux density can be expressed using an Ohm's law analogue that expresses the energy flux density as a product of a network of resistances and a potential difference:

$$H = \frac{\rho_{\mathrm{a}} C_p (T_{\mathrm{s}} - T_{\mathrm{a}})}{R_{\mathrm{a}}} \tag{A6}$$

$$\lambda E = \frac{m_{\mathrm{v}}/m_{\mathrm{v}} \lambda \rho_{\mathrm{a}} (e_{\mathrm{s}}(T_{\mathrm{s}}) - e_{\mathrm{a}})}{P(R_{\mathrm{a}} + R_{\mathrm{s}})}. \tag{A7}$$

In eqs (A6) and (A7), ρ_{a} is air density, λ is the latent heat of vaporization, R_{a} is the aerodynamic conductance for sensible heat transfer (m s^{-1}), R_{s} is stomatal conductance (m s^{-1}), C_p is the specific heat of air (J kg^{-1} K^{-1}), m_{v} and m_{a} are the molecular weights of vapour and dry air (g mol^{-1}), P is pressure (kPa), e_{s} is saturated vapour pressure (kPa) and e_{a} is the ambient vapour pressure (kPa).

Manipulating eqs (A4), (A5) and (A6), and adopting a linearized version of the emission of long-wave radiation ($T_{\mathrm{s}}^4 \sim T_{\mathrm{a}}^4 + 4T_{\mathrm{a}}^3\,(T_{\mathrm{s}} - T_{\mathrm{a}})$) produces an expression for the surface–air temperature difference:

$$T_{\mathrm{s}} - T_{\mathrm{a}} = \frac{Q - \lambda E - \sigma\varepsilon T_{\mathrm{a}}^4 - G_{\mathrm{soil}}}{\rho_{\mathrm{a}} C_p G_{\mathrm{a}} + 4\varepsilon\sigma T_{\mathrm{a}}^3}. \tag{A8}$$

G_{a} is the aerodynamic conductance for heat transfer, the inverse of the resistance ($1/R_{\mathrm{a}}$). Eq. (A8), requires an exact expression for λE too. To obtain an algorithm for λE we linearize the saturation vapour pressure equation with a second-order approximation to Taylor's expansion series:

$$\lambda E = \frac{(m_{\mathrm{v}}/m_{\mathrm{a}})\lambda\rho_{\mathrm{a}} G_{\mathrm{s}} G_{\mathrm{a}}}{P(G_{\mathrm{s}} + G_{\mathrm{a}})} \left((e_{\mathrm{s}}(T_{\mathrm{a}}) - e_{\mathrm{a}}) + s(T_{\mathrm{a}})(T_{\mathrm{s}} - T_{\mathrm{a}}) + \frac{e_{\mathrm{s}}(T_{\mathrm{a}})''}{2}(T_{\mathrm{s}} - T_{\mathrm{a}})^2 \right). \tag{A9}$$

In eq. (A9), G_{s} is surface conductance, s is the slope of the saturation vapour pressure function, $e_{\mathrm{s}}(T)$, with respect to temperature and the double primes represent the second derivative of $e_{\mathrm{s}}(T)$ with respect to T. Finally we combining eqs (A8) and (A9) and substituted an expression that defines the total conductance for vapour transfer, ($G_{\mathrm{w}} = G_{\mathrm{a}} G_{\mathrm{s}}/(G_{\mathrm{a}} + G_{\mathrm{s}})$. This operation produces exact solutions for the coefficients in the quadratic eqs (A1) and (A2). The coefficients for λE are:

$$a = \frac{\rho_{\mathrm{a}}\lambda G_{\mathrm{w}} m_{\mathrm{v}}}{2m_{\mathrm{a}} P(\rho_{\mathrm{a}} C_p G_{\mathrm{a}} + 4\sigma\varepsilon T_{\mathrm{a}}^3)} \frac{\mathrm{d}^2 e_{\mathrm{s}}(T_{\mathrm{a}})}{\mathrm{d}T^2} \tag{A10}$$

$$\begin{aligned} b = {} & -4\varepsilon\sigma T_{\mathrm{a}}^3 - \frac{\rho_{\mathrm{a}}\lambda G_{\mathrm{w}} m_{\mathrm{v}}}{m_{\mathrm{a}} P} \frac{\mathrm{d}e_{\mathrm{s}}(T_{\mathrm{a}})}{\mathrm{d}T} - \rho_{\mathrm{a}} C_p G_{\mathrm{a}} \\ & + \frac{\rho_{\mathrm{a}}\lambda G_{\mathrm{w}} m_{\mathrm{v}}}{2m_{\mathrm{a}} P(\rho_{\mathrm{a}} C_p G_{\mathrm{a}} + 4\sigma\varepsilon T_{\mathrm{a}}^3)} \\ & \times \frac{\mathrm{d}^2 e_{\mathrm{s}}(T_{\mathrm{a}})}{\mathrm{d}T^2} \left(-2Q + 2\sigma\varepsilon T_{\mathrm{a}}^4 + 2G_{\mathrm{soil}}\right) \end{aligned} \tag{A11}$$

$$\begin{aligned} c = {} & \left(\rho_{\mathrm{a}} C_p G_{\mathrm{a}} + 4\varepsilon\sigma T_{\mathrm{a}}^3\right) \frac{\rho_{\mathrm{a}}\lambda G_{\mathrm{w}} m_{\mathrm{v}} (e_{\mathrm{s}}(T_{\mathrm{a}}) - e_{\mathrm{a}})}{m_{\mathrm{a}} P} \\ & + \frac{\rho_{\mathrm{a}}\lambda G_{\mathrm{w}} m_{\mathrm{v}}}{m_{\mathrm{a}} P} \frac{\mathrm{d}e_{\mathrm{s}}(T_{\mathrm{a}})}{\mathrm{d}T} \left(Q - \varepsilon\sigma T_{\mathrm{a}}^4 - G_{\mathrm{soil}}\right) \\ & + \frac{\rho_{\mathrm{a}}\lambda G_{\mathrm{w}} m_{\mathrm{v}}}{2m_{\mathrm{a}} P\left(\rho_{\mathrm{a}} C_p G_{\mathrm{a}} + 4\sigma\varepsilon T_{\mathrm{a}}^3\right)} \frac{\mathrm{d}^2 e_{\mathrm{s}}(T_{\mathrm{a}})}{\mathrm{d}T^2} \Big[Q^2 + \left(\sigma\varepsilon T_{\mathrm{a}}^4\right)^2 \\ & + G_{\mathrm{soil}}^2 - 2Q\sigma\varepsilon T_{\mathrm{a}}^4 - 2QG_{\mathrm{soil}} + 2G_{\mathrm{soil}}\sigma\varepsilon T_{\mathrm{a}}^4 \Big]. \end{aligned} \tag{A12}$$

The coefficients for eq. (A2) are defined as:

$$d = 6\varepsilon\sigma T_{\mathrm{a}}^2 + \frac{\rho_{\mathrm{a}}\lambda G_{\mathrm{w}} m_{\mathrm{v}}}{2m_{\mathrm{a}} P} \frac{\mathrm{d}^2 e_{\mathrm{s}}(T_{\mathrm{a}})}{\mathrm{d}T^2} \tag{A13}$$

$$e = 4\varepsilon\sigma T_{\mathrm{a}}^3 + \frac{\rho_{\mathrm{a}}\lambda G_{\mathrm{w}} m_{\mathrm{v}}}{m_{\mathrm{a}} P} \frac{\mathrm{d}e_{\mathrm{s}}(T_{\mathrm{a}})}{\mathrm{d}T} + \rho C_p G_{\mathrm{a}} \tag{A14}$$

$$f = \varepsilon\sigma T_{\mathrm{a}}^4 + \frac{\rho_{\mathrm{a}}\lambda G_{\mathrm{a}} m_{\mathrm{v}} (e_{\mathrm{s}}(T_{\mathrm{a}}) - e_{\mathrm{a}})}{m_{\mathrm{a}} P} + -Q + G_{\mathrm{soil}}. \tag{A15}$$

References

Ackland, G. J., Clark, M. A. and Lenton, T. M. 2003. Catastrophic desert formation in Daisyworld. *J. Theor. Biol.* **223**, 39–44.

Adams, B., Carr, J., Lenton, T. M. and White, A. 2003. One-dimensional daisyworld: spatial interactions and pattern formation. *J. Theor. Biol.* **223**, 505–513.

Avissar, R. 1995. Scaling of land–atmosphere interactions-an atmospheric modeling perspective. *Hydrol. Process.* **9**, 679–695.

Baldocchi, D. D. 2003. Assessing the eddy covariance technique for evaluating carbon dioxide exchange rates of ecosystems: past, present and future. *Global Change Biol* **9**, 479–492.

Baldocchi, D. D., Falge, E., Gu, L. H., Olson, R., Hollinger, D. and co-authors. 2001. FLUXNET: a new tool to study the temporal and spatial variability of ecosystem-scale carbon dioxide, water vapor, and energy flux densities. *Bull. Am. Meteorol. Soc.* **82**, 2415–2434.

Baldocchi, D. D., Fuentes, J., Bowling, D., Turnipseed, A. and Monson, R. 1999. Scaling isoprene fluxes from leaves to canopies: test cases over a boreal aspen and a mixed temperate forest. *J. Appl. Meteorol.* **38**, 885–898.

Baldocchi, D. D. and Meyers, T. 1998. On using eco-physiological, micrometeorological and biogeochemical theory to evaluate carbon dioxide, water vapor and trace gas fluxes over vegetation: a perspective. *Agric. Forest Meteorol.* **90**, 1–25.

Baldocchi, D. D. and Rao, K. S. 1995. Intra-field variability of scalar flux densities across a transition between a desert and an irrigated potato advection field. *Boundary Layer Meterol.* **76**, 109–136.

Baldocchi, D. D., Xu, L. and Kiang, N. 2004. How plant functional-type, weather, seasonal drought, and soil physical properties alter water and energy fluxes of an oak-grass savanna and an annual grassland. *Agric. Forest Meteorol.* **123**, 13–39.

Bonan, G. B., Pollard, D. and Thompson, S. L. 1993. Influence of subgrid scale heterogeneity in leaf area index, stomatal resistance and soil moisture on grid scale land-atmosphere interactions. *J. Climate* **6**, 1882–1897.

Brunsell, N. A. and Gillies, R. R. 2003. Scale issues in land-atmosphere interactions: implications for remote sensing of the surface energy balance. *Agric. Forest Meteorol.* **117**, 203–221.

Bunzli, D. and Schmid, H. P. 1998. The influence of surface texture on regionally aggregated evaporation and energy partitioning. *J. Atmos. Sci.* **55**, 961–972.

Canadell, J., Mooney, H., Baldocchi, D., Berry, J., Ehleringer, J. and co-authors. 2000. Carbon metabolism of the terrestrial biosphere. *Ecosystems* **3**, 115–130.

Cohen, J. E. and Rich, A. D. 2000. Interspecific competition affects temperature stability in Daisyworld. *Tellus B* **52**, 980–984.

Crawford, T., Dobosy, R., McMillen, R., Vogel, C. and Hicks, B. 1996. Air-surface exchange measurement in heterogeneous regions: extending tower observations with spatial structure observed from small aircraft. *Global Change Biol.* **2**, 275–285.

Cronhort, M. B. 2000. The interplay between reaction and diffusion. In: *The Geometry of Ecological Interactions: Simplifying Spatial Complexity* (eds U. Dieckmann, R. Law and J. Metz), pp. 151–170. Cambridge University Press, Cambridge.

Desjardins, R. L., MacPherson, J. I., Mahrt, L., Schuepp, P., Pattey, E. and co-authors. 1997. Scaling up flux measurements for the boreal forest using aircraft-tower combinations. *J. Geophys. Res.* **102**, 29 125–29 134.

Dickinson, R. E. 1995. Land processes in climate models. *Remote Sensing Environ.* **51**, 27–38.

Eagleson, P. J. 1982. Ecological optimality in water limited natural soil-vegetation systems. *Water Resour. Res.* **18**, 325–340.

Fernandez-Illescas, C. P. and Rodriguez-Iturbe, I. 2004. The impact of interannual rainfall variability on the spatial and temporal patterns of vegetation in a water-limited ecosystem. *Adv. Water Resour.* **27**, 83–95.

Gardner, M. 1971. Cellular automata, self-reproduction, garden of Eden and Game of Life. *Sci. Am.* **224**, 112.

Higgins, S. I., Bond, W. J. and Trollope, W. S. W. 2000. Fire, resprouting and variability: a recipe for grass-tree coexistence in savanna. *J. Ecol.* **88**, 213–229.

Jeltsch, F., Milton, S. J., Dean, W. R. J. and van Rooyen, N. 1996. Tree spacing and coexistence in semiarid savannas. *J. Ecol.* **84**, 583–595.

Kim, J., Guo, Q., Baldocchi, D., Xu, L., Leclerc, M. and co-authors. 2005. Upscaling CO2 fluxes from tower to landscape: overlaying tower flux footprint calculations on high resolution (IKONOS) vegetation density images. *Agric. Forest Meteorol.* in press.

Kustas, W. P., Norman, J. M., Anderson, M. C. and French, A. N. 2003. Estimating subpixel surface temperatures and energy fluxes from the vegetation index-radiometric temperature relationship. *Remote Sensing Environ.* **85**, 429–440.

Lenton, T. M. and Lovelock, J. E. 2001. Daisyworld revisited: quantifying biological effects on planetary self-regulation. *Tellus* **53B**, 288–305.

Lenton, T. M. and van Oijen, M. 2002. Gaia as a complex adaptive system. *Phil. Trans. R. Soc. Lond. B* **357**, 683–695.

Levin, S. A. 1992. The problem of pattern and scale in ecology. *Ecology* **73**, 1943–1967.

Lyons, T. J. and Halldin, S. 2004. Surface heterogeneity and the spatial variation of fluxes. *Agric. Forest Meteorol.* **121**, 153–165.

McGuffie, K. and Henderson-Sellers, A. 1997. *A Climate Modeling Primer*. 2nd edn. Wiley, Chichester.

McNaughton, K. G. 1994. Effective stomatal and boundary-layer resistances of heterogeneous surfaces. *Plant Cell Environ.* **17**, 1061–1068.

Monteith, J. L. and Unsworth, M. H. 1990. *Principles of Environmental Physics*, Edward Arnold, London.

Morisette, J. T., Nickeson, J. E., Davis, P., Wang, Y., Tian, Y. and co-authors. 2003. High spatial resolution satellite observations for validation of MODIS land products: IKONOS observations acquired under the NASA scientific data purchase. *Remote Sensing Environ.* **88**, 100–110.

Nilson, T. 1971. A theoretical analysis of the frequency of gaps in plant stands. *Agric. Meteorol.* **8**, 25–38.

Ogunjemiyo, S. O., Kaharabata, S. K., Schuepp, P. H., MacPherson, I. J., Desjardins, R. L. and co-authors. 2003. Methods of estimating CO2, latent heat and sensible heat fluxes from estimates of land cover fractions in the flux footprint. *Agric. Forest Meteorol.* **117**, 125–144.

Park, Y.-S. and Paw U, K. T. 2004. Numerical estimation of horizontal advection inside canopies. *J. Appl. Meteorol.* **43**, 1530–1538.

Paw U, K. T. and Gao, W. 1988. Applications of solutions to non-linear energy budget equations. *Agric. Forest Meteorol.* **43**, 121–145.

Pielke, R. A. Sr., Avissar, R., Raupach, M., Dolman, A. J. and co-authors. 1998. Interactions between the atmosphere and terrestrial ecosystems: influence on weather and climate. *Global Change Biol.* **4**, 461–475.

Press, W. H., Teukolsky, S. A., Vetterling, W. T. and Flannery, B. P. 1988. *Numerical Recipes in C*. Cambridge University Press, Cambridge.

Pyles, R. D., Weare, B. C., Paw U, K. T. and Gustafson, W. 2003. Coupling between the University of California, Davis, Advanced Canopy–Atmosphere–Soil Algorithm (ACASA) and MM5: preliminary results for July 1998 for western North America. *J. Appl. Meteorol.* **42**, 557–569.

Raupach, M. R. 1991. Vegetation–atmosphere interaction in homogeneous and heterogeneous terrain—some implications of mixed-layer dynamics. *Vegetatio* **91**, 105–120.

Raupach, M. R. and Finnigan, J. J. 1995. Scale issues in boundary layer meteorology-surface energy balances in heterogeneous terrain. *Hydrol. Process.* **9**, 589–612.

Rietkerk, M., Dekker, S. C., de Ruiter, P. C. and van de Koppel, J. 2004. Self-organized patchiness and catastrophic shifts in ecosystems. *Science* **305**, 1926–1929.

Rodriguez-Iturbe, I., D'Odorico, P., Porporato, A. and Ridolfi, L. 1999. Tree-grass coexistence in savannas: the role of spatial dynamics and climate fluctuations. *Geophys. Res. Lett.* **26**, 247–250.

Running, S. W., Baldocchi, D. D., Turner, D., Gower, S. T., Bakwin, P. and co-authors. 1999. A global terrestrial monitoring network, scaling tower fluxes with ecosystem modeling and EOS satellite data. *Remote Sensing Environ.* **70**, 108–127.

Running, S. W., Loveland, T. R., Pierce, L. L., Nemani, R. R. and Hunt, J. E. R. 1995. A remote sensing based vegetation classification logic for global land cover analysis 1. *Remote Sensing Environ.* **51**, 39–48.

Running, S., Nemani, R., Heinsch, F., Zhao, M., Reeves, M. and co-authors. 2004. A continuous satellite-derived measure of global terrestrial primary production. *BioScience* **54**, 547–560.

Sankaran, M., Ratnam, J. and Hanan, N. P. 2004. Tree-grass coexistence in savannas revisited—insights from an examination of assumptions and mechanisms invoked in existing models. *Ecol. Lett.* **7**, 480–490.

Saunders, P. T. 1994. Evolution without natural selection: further implications of the Daisyworld parable. *J. Theor. Biol.* **166**, 365–373.

Schmid, H. P. 2002. Footprint modeling for vegetation atmosphere exchange studies: a review and perspective. *Agric. Forest Meteorol.* **113**, 159–183.

Scholes, R. J. and Archer, S. R. 1997. Tree–grass interactions in savannas. *Annu. Rev. Ecol. Syst.* **28**, 517–544.

Sellers, P. J. 1987. Canopy reflectance, photosynthesis, and transpiration, II. The role of biophysics in the linearity of their interdependence. *Remote Sensing Environ.* **21**, 143–183.

Sellers, P. J., Dickinson, R. E., Randall, D. A., Betts, A. K., Hall, F. G. and co-authors. 1997. Modeling the exchanges of energy, water, and carbon between continents and the atmosphere. *Science* **275**, 502–509.

Ustin, S. L., Roberts, D. A., Gamon, J. A., Asner, G. P. and Green, R. O. 2004. Using imaging spectroscopy to study ecosystem processes and properties. *BioScience* **54**, 523–534.

van Wijk, M. T. and Rodriguez-Iturbe, I. 2002. Tree–grass competition in space and time: insights from a simple cellular automata model based on ecohydrological dynamics. *Water Resour. Res.* **38**(9), 1179, doi:10.1029/2001WR000768.

von Bloh, W., Block, A. and Schellnhuber, H. J. 1997. Self-stabilization of the biosphere under global change: a tutorial geophysiological approach. *Tellus B* **49**, 249–262.

von Bloh, W., Block, A., Parade, M. and Schellnhuber, H. J. 1999. Tutorial modelling of geosphere–biosphere interactions: the effects of percolation-type habitat fragmentation. *Physica A* **266**, 186–196.

Watson, A. and Lovelock, J. 1983. Biological homeostasis of the global environment: the parable of Daisyworld. *Tellus* **35B**, 286–289.

Wilson, K., Goldstein, A., Falge, E., Aubinet, M., Baldocchi, D. and co-authors. 2002. Energy balance closure at FLUXNET sites. *Agric. Forest Meteorol.* **113**, 223–243.

Wolfram, S. 2002. *A New Kind of Science*. Wolfram Media, Champaign, IL.

Zeng, X., Pielke, R. A. and Eykholt, R. 1990. Chaos in Daisyworld. *Tellus* **42B**, 309–318.